

Article

# Second-Order Model-Based Predictive Control of Dual Three-Phase PMSM Based on Current Loop Operation Optimization

Long Li <sup>1,2</sup>, Weidong Zhou <sup>1,\*</sup>, Xianting Bi <sup>3</sup>, Xuetao Sun <sup>4</sup> and Xiaoping Shi <sup>5</sup><sup>1</sup> College of Intelligent Systems Science and Engineering, Harbin Engineering University, Harbin 150006, China<sup>2</sup> School of Electrical and Electronic Engineering, Harbin University of Science and Technology, Harbin 150080, China<sup>3</sup> Beijing Institute of Astronautics System Engineering, Beijing 100076, China<sup>4</sup> Institute of Smart City, Shanghai University, Shanghai 200444, China<sup>5</sup> School of Astronautics, Harbin Institute of Technology, Harbin 150080, China

\* Correspondence: zhouweidong@hrbeu.edu.cn; Tel.: +86-0451-82568107

**Abstract:** To reduce the amount of computation in traditional model predictive current control, to improve the flexibility in choosing the direction and amplitude in the voltage vector synthesis of a dual three-phase motor by two degrees of freedom, and to reduce the output torque ripple and current ripple, this paper proposes a dual second-order model predictive control algorithm based on current loop operation optimization. Compared with the conventional speed loop using the PI control algorithm and the traditional MPC control algorithm, the proposed algorithm adopts the second-order MPC control mode in the speed loop, which decreases the speed regulation time and increases motor immunity. Meanwhile, the second-order MPC control mode is adopted in the current loop, and the traditional iterative calculation method is improved to calculate the direction and amplitude of the output voltage vector through the analytic function, which increases the flexibility of the output voltage vector. Additionally, a four-vector SVPWM is employed to modulate the voltage vector to reduce the current amplitude in the harmonic subspace. The simulation results indicate that the algorithm proposed in this paper can significantly reduce the torque ripple and the current ripple as well as increase the transient performance of the motor.

**Keywords:** dual three-phase permanent magnet synchronous motor; dual second-order model predictive control; current loop optimization; iterative optimization



**Citation:** Li, L.; Zhou, W.; Bi, X.; Sun, X.; Shi, X. Second-Order Model-Based Predictive Control of Dual Three-Phase PMSM Based on Current Loop Operation Optimization. *Actuators* **2022**, *11*, 251. <https://doi.org/10.3390/act11090251>

Academic Editor: Paolo Mercorelli

Received: 2 August 2022

Accepted: 29 August 2022

Published: 1 September 2022

**Publisher's Note:** MDPI stays neutral with regard to jurisdictional claims in published maps and institutional affiliations.



**Copyright:** © 2022 by the authors. Licensee MDPI, Basel, Switzerland. This article is an open access article distributed under the terms and conditions of the Creative Commons Attribution (CC BY) license (<https://creativecommons.org/licenses/by/4.0/>).

## 1. Introduction

The multi-phase motor drive system featured low voltage and high-power output, low torque ripple, high-operation reliability, and high-control flexibility. It has good application prospects in many fields, such as electric vehicles, metallurgical steel rolling, and electric ship propulsion [1].

The control algorithms for multi-phase motors are mainly divided into three categories, namely vector control, direct torque control, and model predictive control (MPC) [1]. Among them, MPC can handle multi-input and multi-output nonlinear systems with complex constraints and has superior dynamic performance and parameter robustness. Numerous studies have been conducted on the application of MPC in motor drive systems [2–6]. The traditional MPC conducts rolling optimization on the control variables and selects the voltage vector with the minimum objective function value as the optimal solution for the output. Meanwhile, the process of traversing each voltage vector requires a large amount of calculation. Compared with the traditional three-phase motor, the multi-phase motor involves more voltage vectors geometrically, and the calculation amount also increases. For the limited number of voltage vectors and uncertainty conduction sequences,

the current harmonic will deteriorate; Reference [7] proposed a simplified model predictive torque control, in which the harmonic currents were suppressed effectively, and the computational burden can be alleviated.

Y. Luo et al. [8] proposed multi-channel voltage control based on reference voltage vectors. To suppress current harmonics, 24 groups of virtual voltage vectors were defined, thereby reducing the computational burden. Then, based on Reference [8], a six-phase motor MPC with a reduced-dimension cost function was proposed, which simplified the prediction model and effectively suppressed the harmonic current [9]. X. Sun et al. [10] proposed 24 new virtual voltage vectors that do not need to adjust MPC weighting factors. J. J. Aciego et al. [11] proposed a six-phase motor with predictive control and two virtual voltage vectors, which limited the appearance of secondary currents, improved the accuracy of control actions, and [12] provided a proof study for AC machines with traditional predictive current control. Waleed A et al. [13] proposed adopting virtual space vector-based MPC for the three-level T-type converters inherent in DC-link voltage balancing, in which the proposed approach not only simplified the controller design by using a simplified cost function but also reduced the execution time of MPC significantly. Based on Reference [12], Guo et al. added the duty cycle control method to adjust the amplitude of the output voltage vectors and to suppress the current and torque ripple. However, this still could not adjust the direction of the voltage vectors. M.J. Duran et al. [13] proposed a novel, constrained search-predictive control algorithm that utilized more basic voltage vectors. Although the algorithm can increase the degree of freedom of the control vectors and improve the dynamic performance of the motor, it increases the amount of computation. A. Taheri et al. [14] proposed a Kalman filter-based predictive control for six-phase motors, which ensured robustness amidst parameter uncertainty and external disturbances.

In traditional MPC, optimizing the voltage vector takes a substantial amount of time during the current loop rolling optimization process. For the dual three-phase permanent magnet synchronous motor, the number of voltage vectors is a multiple of the three-phase PMSM; it is difficult for MPC to complete optimization in one PWM period. Aiming to solve this problem, this study proposes a dual second-order model predictive control algorithm based on current loop operation optimization. The proposed algorithm can calculate the direction and amplitude of the output voltage vector in the next time step using only one calculation. This increases the flexibility of the output voltage vector, reduces the content of current harmonics, and reduces the number of MPC loop computations. Meanwhile, to reduce the current amplitude in the harmonic subspace, the maximum four-vector SVPWM was used to modulate the calculated optimal voltage vector. To further improve the transient performance of the motor, both the speed loop and the current loop are replaced by the MPC regulation control algorithm using the second-order discrete model. Finally, simulation results prove the feasibility and validity of the proposed algorithm.

## 2. Mathematical Model of Dual Three-Phase Permanent Magnet Synchronous Motor

This study takes the hidden-pole dual three-phase permanent magnet synchronous motor as the research object. Its stator is composed of two sets of three-phase windings with a phase shift of  $30^\circ$  in space. The neutral points of the windings are not connected, and the three-phase windings are spatially separated by an electrical angle of  $120^\circ$ . The drive circuit is a two-level six-arm inverter. The topology diagram of the research object is shown in Figure 1.

To facilitate the analysis, this study adopts the method of space vector decoupling coordinate transformation. Meanwhile, the principle of constant amplitude transformation is employed to transform the variables in the natural coordinate system of the dual three-phase motor into three mutually orthogonal subspaces. The transformation equation is as follows:

$$[h_\alpha h_\beta h_x h_y h_{o1} h_{o2}]^T = T_1 [h_A h_B h_C h_U h_V h_W]^T \quad (1)$$

where  $h_A, h_B, h_C, h_U, h_V,$  and  $h_W$  are the variables of the six-phase natural coordinate system;  $h_\alpha$  and  $h_\beta$  are the variables of the  $\alpha - \beta$  subspace;  $h_x$  and  $h_y$  are the variables of

the  $x - y$  subspace;  $h_{o1}$  and  $h_{o2}$  are the variables of the  $o1 - o2$  subspace; and  $T_1$  is the transformation matrix, which can be represented as

$$T_1 = \frac{1}{3} \begin{bmatrix} 1 & -\frac{1}{2} & -\frac{1}{2} & \frac{\sqrt{3}}{2} & -\frac{\sqrt{3}}{2} & 0 \\ 0 & \frac{\sqrt{3}}{2} & -\frac{\sqrt{3}}{2} & \frac{1}{2} & \frac{1}{2} & -1 \\ 1 & -\frac{1}{2} & -\frac{1}{2} & -\frac{\sqrt{3}}{2} & \frac{\sqrt{3}}{2} & 0 \\ 0 & -\frac{\sqrt{3}}{2} & \frac{\sqrt{3}}{2} & \frac{1}{2} & \frac{1}{2} & -1 \\ 1 & 1 & 1 & 0 & 0 & 0 \\ 0 & 0 & 0 & 1 & 1 & 1 \end{bmatrix} \quad (2)$$

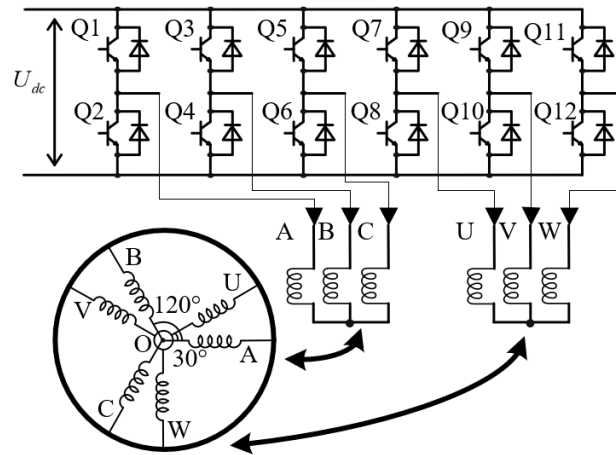


Figure 1. Dual three-phase permanent magnet synchronous motor and its drive circuit.

The components in the  $\alpha - \beta$  subspace participate in electromechanical energy conversion. The components in the  $x - y$  subspace do not participate in the electromechanical energy conversion and cause energy loss. The components in the  $o1 - o2$  subspace are zero-sequence components. Since the neutral points of the two sets of three-phase windings in this study are not connected, the zero-sequence components do not exist. Thus, only the  $\alpha - \beta$  subspace and the  $x - y$  subspace can be analyzed. The voltage equation after the above coordinate transformation is expressed as

$$\begin{cases} v_\alpha = R_s i_\alpha + L_\alpha \frac{di_\alpha}{dt} - \omega_e \psi_f \sin(\theta_e) \\ v_\beta = R_s i_\beta + L_\beta \frac{di_\beta}{dt} + \omega_e \psi_f \cos(\theta_e) \\ v_x = R_s i_x + L_l \frac{di_x}{dt} \\ v_y = R_s i_y + L_l \frac{di_y}{dt} \end{cases} \quad (3)$$

where  $v_\alpha$ ,  $v_\beta$ ,  $v_x$ , and  $v_y$  are voltage components of the  $\alpha - \beta$  and  $x - y$  subspaces;  $i_\alpha$ ,  $i_\beta$ ,  $i_x$ , and  $i_y$  are current components of the  $\alpha - \beta$  and  $x - y$  subspaces;  $L_\alpha$  and  $L_\beta$  are inductances of the  $\alpha$ - and  $\beta$ -axes;  $L_l$  is leakage induction, and  $L_\alpha = L_\beta = L_l + 3L_m$  ( $L_m$  is self-inductance);  $\omega_e$  is the rotor electric angular velocity;  $\theta_e$  is the electrical angle of the rotor relative to the phase A axis in the counterclockwise direction;  $\psi_f$  is the rotor permanent magnet flux linkage; and  $R_s$  is the stator resistance.

### 3. The Principle of MPC and Model Establishment

#### 3.1. Establishment of a Prediction Model for Dual Three-Phase PMSM

As shown in Reference [11], if the speed loop and the current loop are combined into a link and the MPC control strategy is adopted, the dynamic response of the motor can be enhanced, but the complexity of the objective function will be increased. To reduce the complexity of the objective function, this study adopts the cascade scheme; that is, the speed loop and the current loop are cascaded. The PID control algorithm is widely used because of its simple structure and easy adjustment [12]. By using the PID control algorithm for speed loop regulation and cascading the latter-stage current loop MPC algorithm, a conventional dual three-phase PMSM dual-loop regulation drive system can be established, as shown in Figure 2. The system includes the speed outer loop controlled by PI and the current inner loop controlled by MPC. The output of the speed loop is used as the given value of the current of the  $q$  axis in the current loop. Additionally, the given values of the current of the  $d$ -,  $x$ -, and  $y$ -axes are set to 0. By calculating MPC in one time step, the PWM waveform is output. Meanwhile, the six-phase inverter bridge is controlled to drive the dual three-phase PMSM so that the actual current of the motor tracks the given value of the current loop.

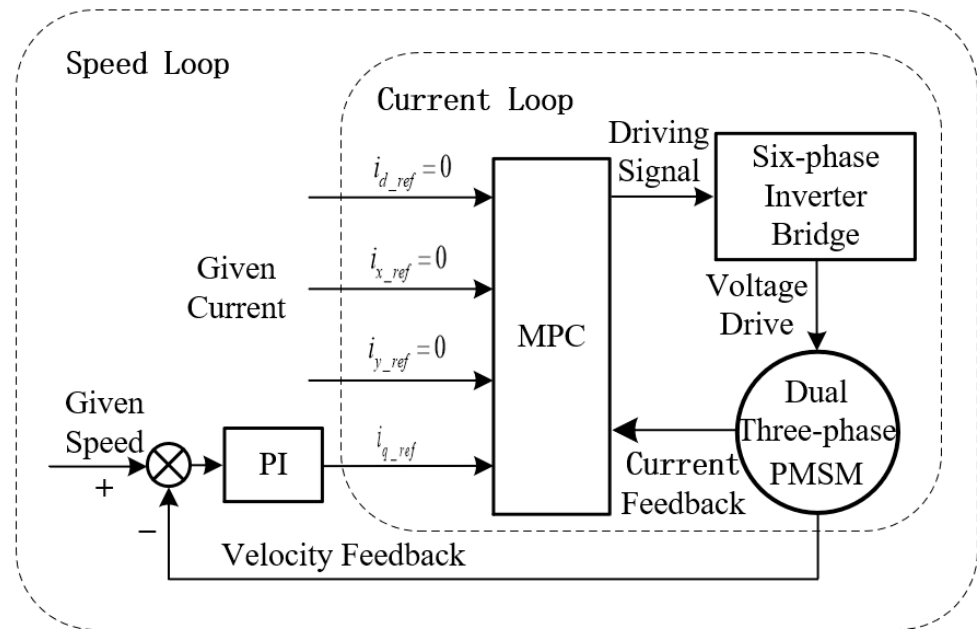


Figure 2. A conventional dual three-phase PMSM drive system.

To facilitate the analysis, the first-order forward Euler discretization is performed on Equation (3), and the result is represented as

$$\begin{cases} i_{\alpha}^{k+1} = \frac{(L_{\alpha} - R_s T_s)}{L_{\alpha}} i_{\alpha}^k + \frac{T_s v_{\alpha}^k + \omega_r^k T_s \psi_f \sin(\theta_e^k)}{L_{\alpha}} \\ i_{\beta}^{k+1} = \frac{(L_{\beta} - R_s T_s)}{L_{\beta}} i_{\beta}^k + \frac{T_s v_{\beta}^k - \omega_r^k T_s \psi_f \cos(\theta_e^k)}{L_{\beta}} \\ i_x^{k+1} = \frac{(L_l - R_s T_s)}{L_l} i_x^k + \frac{T_s v_x^k}{L_l} \\ i_y^{k+1} = \frac{(L_l - R_s T_s)}{L_l} i_y^k + \frac{T_s v_y^k}{L_l} \end{cases} \quad (4)$$

where  $i_{\alpha}^k, i_{\beta}^k, i_x^k, i_y^k, i_{\alpha}^{k+1}, i_{\beta}^{k+1}, i_x^{k+1},$  and  $i_y^{k+1}$  are current components of  $\alpha - \beta$  and  $x - y$  subspaces at time  $k$  and  $k+1$ , respectively;  $T_s$  is the calculation sampling period.

Then, Equation (4) is written as

$$\begin{cases} i_{\alpha}^{k+1} = k_1 v_{\alpha}^k + b_1^k \\ i_{\beta}^{k+1} = k_1 v_{\beta}^k + b_2^k \\ i_x^{k+1} = k_2 v_x^k + b_3^k \\ i_y^{k+1} = k_2 v_y^k + b_4^k \end{cases} \quad (5)$$

where  $k_1 = T_s/L_{\alpha} = T_s/L_{\beta}$ , and  $k_2 = T_s/L_l$ ,

$$b_1^k = [(L_{\alpha} - R_s T_s) i_{\alpha}^k + \omega_e^k T_s \psi_f \sin(\theta_e^k)] / L_{\alpha},$$

$$b_2^k = [(L_{\beta} - R_s T_s) i_{\beta}^k - \omega_e^k T_s \psi_f \cos(\theta_e^k)] / L_{\beta},$$

$$b_3^k = (L_l - R_s T_s) i_x^k / L_l, \quad b_4^k = (L_l - R_s T_s) i_y^k / L_l.$$

The objective function is selected as

$$\begin{aligned} J_1^k = & \mu_1 (i_{\alpha\_ref}^k - i_{\alpha\_pre}^{k+1})^2 + \mu_2 (i_{\beta\_ref}^k - i_{\beta\_pre}^{k+1})^2 \\ & + \mu_3 (i_{x\_ref}^k - i_{x\_pre}^{k+1})^2 + \mu_4 (i_{y\_ref}^k - i_{y\_pre}^{k+1})^2 \end{aligned} \quad (6)$$

where  $J_1^k$  is the objective function at time  $k$ ;  $\mu_1, \mu_2, \mu_3$ , and  $\mu_4$  are weight coefficients;  $i_{\alpha\_ref}^k, i_{\beta\_ref}^k, i_{x\_ref}^k$ , and  $i_{y\_ref}^k$  are the reference currents of  $\alpha - \beta$  and  $x - y$  subspaces at time  $k$ ; and  $i_{\alpha\_pre}^{k+1}, i_{\beta\_pre}^{k+1}, i_{x\_pre}^{k+1}$ , and  $i_{y\_pre}^{k+1}$  are the predicted currents of the corresponding components at time  $k + 1$ .

In the conventional model predictive current control of the dual three-phase permanent magnet synchronous motor, 1 of the 48 independent voltage vectors and 0 vectors in the  $\alpha - \beta$  subspace (Figure 3) are usually selected as the voltage vector that minimizes the objective function, and it is output after the calculation of the current time step. As a result, 49 loop computations will be performed in the current time step calculation process, and the calculation amount is large. However, the limitation of the number of selectable voltage vectors leads to a large output torque ripple. Additionally, since only one voltage vector is selected and the voltage vectors of the  $x - y$  subspace are not controlled, the current in the  $x - y$  subspace is large and the motor loss is high.

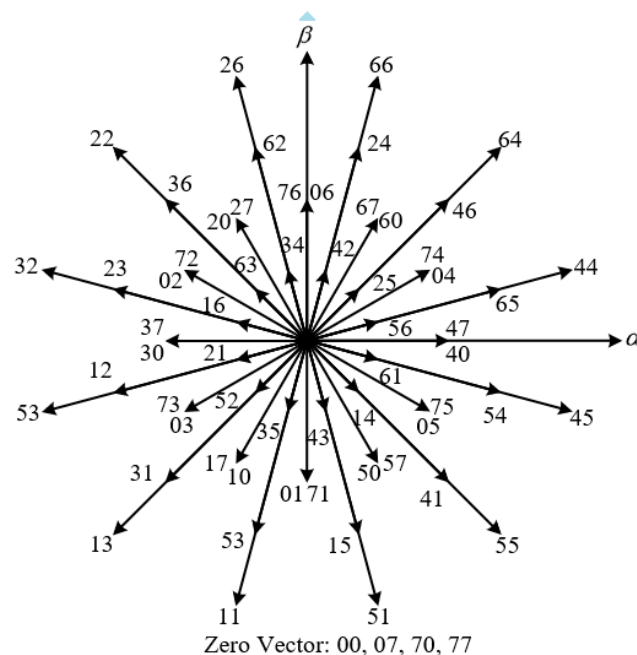


Figure 3. Voltage vector distribution in the  $\alpha - \beta$  subspace.

### 3.2. First-Order Model Predictive Current Control Based on Four-Vector SVPWM

This study adopts the maximum four-vector SVPWM modulation technique in Reference [13] for the voltage calculated by the current MPC. Since the voltage synthesis vector of the  $x - y$  subspace of the four-vector SVPWM is 0, only the  $\alpha - \beta$  subspace can be analyzed. Then, the objective function in Equation (6) can be transformed into

$$J_2^k = \mu_1 \left( i_{\alpha\_ref}^k - i_{\alpha\_pre}^{k+1} \right)^2 + \mu_2 \left( i_{\beta\_ref}^k - i_{\beta\_pre}^{k+1} \right)^2 \quad (7)$$

By taking  $\mu_1 = \mu_2 = 1$  and substituting it into Equation (7), we have

$$J_{2'}^k = \frac{J_2^k}{k^2} = \left( v_{\alpha}^k - \frac{c_1^k}{k} \right)^2 + \left( v_{\beta}^k - \frac{c_2^k}{k} \right)^2 \quad (8)$$

where  $c_1^k = i_{\alpha\_ref}^k - b_1^k$  and  $c_2^k = i_{\beta\_ref}^k - b_2^k$ .

In the maximum four-vector SVPWM linear modulation region, the maximum composite voltage vector amplitude of the  $\alpha - \beta$  plane is  $0.577U_{dc}$  ( $U_{dc}$  is the DC bus voltage of the drive bridge). Hence, the constraint condition of the objective function is

$$(v_{\alpha}^k)^2 + (v_{\beta}^k)^2 \leq (0.577U_{dc})^2 \quad (9)$$

To minimize  $J_{2'}^k$ , there can be two cases.

One case is when  $(c_1^k/k)^2 + (c_2^k/k)^2 \leq (0.577U_{dc})^2$ ,  $v_{\alpha}^k = c_1^k/k$ , and  $v_{\beta}^k = c_2^k/k$  are taken. The other case is when  $(c_1^k/k)^2 + (c_2^k/k)^2 > (0.577U_{dc})^2$ , the nearest intersection point of the circle  $(v_{\alpha}^k)^2 + (v_{\beta}^k)^2 = (0.577U_{dc})^2$ , and the coordinate  $(v_{\alpha}^k, v_{\beta}^k) = (c_1^k/k, c_2^k/k)$  are taken, that is, to solve the following equation group:

$$\begin{cases} v_{\beta}^k = \frac{c_2^k/k}{c_1^k/k} v_{\alpha}^k \\ (v_{\alpha}^k)^2 + (v_{\beta}^k)^2 = (0.577U_{dc})^2 \end{cases} \quad (10)$$

The two solutions are as follows.

$$\begin{cases} v_{\alpha}^k(1) = 0.577U_{dc} \sqrt{\frac{(c_1^k)^2}{(c_1^k)^2 + (c_2^k)^2}} \\ v_{\beta}^k(1) = 0.577U_{dc} \frac{c_2^k}{c_1^k} \sqrt{\frac{(c_1^k)^2}{(c_1^k)^2 + (c_2^k)^2}} \end{cases} \quad (11)$$

$$\begin{cases} v_{\alpha}^k(2) = -0.577U_{dc} \sqrt{\frac{(c_1^k)^2}{(c_1^k)^2 + (c_2^k)^2}} \\ v_{\beta}^k(2) = -0.577U_{dc} \frac{c_2^k}{c_1^k} \sqrt{\frac{(c_1^k)^2}{(c_1^k)^2 + (c_2^k)^2}} \end{cases} \quad (12)$$

The coordinates  $(v_{\alpha}^k(1), v_{\beta}^k(1))$  and  $(v_{\alpha}^k(2), v_{\beta}^k(2))$  with the closest linear distance to the coordinate  $(c_1^k/k, c_2^k/k)$  is taken as the output  $v_{\alpha}^k$  and  $v_{\beta}^k$  of the MPC at this time step, i.e., the given value of the maximum four-vector SVPWM. This output is the MPC control output using the first-order discrete voltage model.

### 3.3. Second-Order Model Predictive Current Control Based on Four-Vector SVPWM

To improve the current tracking performance, the above voltage equation is modified into a second-order form by changing the first two terms of Equation (5) into

$$\begin{cases} i_{\alpha}^{k+1} = k_1 v_{\alpha}^k + b_1^k \\ i_{\alpha}^k = k_1 v_{\alpha}^{k-1} + b_1^{k-1} \\ i_{\beta}^{k+1} = k_1 v_{\beta}^k + b_2^k \\ i_{\beta}^k = k_1 v_{\beta}^{k-1} + b_2^{k-1} \end{cases} \quad (13)$$

By further organization, we have

$$\begin{cases} i_{\alpha}^{k+1} = k_1 v_{\alpha}^k + d_1^{k-1,k} \\ i_{\beta}^{k+1} = k_1 v_{\beta}^k + d_2^{k-1,k} \end{cases} \quad (14)$$

where

$$\begin{cases} d_1^{k-1,k} = b_1^k - b_1^{k-1} - k_1 v_{\alpha}^{k-1} + i_{\alpha}^k \\ d_2^{k-1,k} = b_2^k - b_2^{k-1} - k_1 v_{\beta}^{k-1} + i_{\beta}^k \end{cases} \quad (15)$$

The above equation is the second-order discrete voltage model. Referring to the previous solution process using the first-order discrete voltage model,  $c_1^k$  is replaced with  $i_{\alpha\_ref}^k - d_1^{k-1,k}$  and  $c_2^k$  is replaced with  $i_{\beta\_ref}^k - d_2^{k-1,k}$ . In this approach, the MPC control output voltage vector can be solved using the second-order discrete voltage model.

### 3.4. Dual Second-Order Model Predictive Current Control Based on Four-Vector SVPWM

In the conventional speed loop, the PI controller is usually selected as the regulator (Figure 2), and its output is used as the given value of the current loop. To improve the dynamic performance and anti-interference ability of the motor, this study replaces the PI controller of the conventional speed loop with the MPC controller using the second-order discrete mechanical equation.

According to the electromagnetic torque equation of the dual three-phase permanent magnet synchronous motor, we have

$$T_e = 3p_n[\psi_f i_q + (L_d - L_q)i_d i_q] \quad (16)$$

where  $T_e$  is the electromagnetic torque;  $p_n$  is the number of motor pole pairs;  $\psi_f$  is the permanent magnet flux linkage;  $i_d$  and  $i_q$  are the current of  $d$  axis and  $q$  axis, respectively; and  $L_d$  and  $L_q$  are the inductance of  $d$  axis and  $q$  axis, respectively.

Since this study takes the hidden-pole dual three-phase motor as the research object, then  $L_d = L_q$ , and the above equation can be changed into

$$T_e = k_t i_q \quad (17)$$

where  $k_t = 3p_n \psi_f$  is denoted as the torque coefficient.

According to the mechanical equation of the dual three-phase permanent magnet synchronous motor, we have

$$T_e - T_L - \omega_r B_m = J \frac{d\omega_r}{dt} \quad (18)$$

where  $T_L$  is the load torque,  $\omega_r$  is the rotor mechanical angular velocity,  $B_m$  is the friction coefficient, and  $J$  is the rotational inertia.

Let  $T_L = 0$ . After conducting the first-order forward Euler discretization on the above equation and organizing the results, we have

$$\omega_r^{k+1} = m_1\omega_r^k + n_1i_q^k \tag{19}$$

where  $m_1 = (J - B_m T_s)/J$  and  $n_1 = T_s k_t / J$ .

From the above equation, there is

$$\omega_r^k = m_1\omega_r^{k-1} + n_1i_q^{k-1} \tag{20}$$

Combined with equations (19) and (20), the following equation can be obtained.

$$\omega_r^{k+1} = (1 + m_1)\omega_r^k - m_1\omega_r^{k-1} + n_1i_q^k - n_1i_q^{k-1} \tag{21}$$

Then the model-predicted rotational speed equation of the second-order discrete mechanical equation can be obtained:

$$\omega_{r\_pre}^{k+1} = (1 + m_1)\omega_r^k - m_1\omega_r^{k-1} + n_1i_q^k - n_1i_q^{k-1} \tag{22}$$

where  $\omega_{r\_pre}^{k+1}$  is the predicted speed at time  $k + 1$ .

Then, the given current  $i_{q\_ref}^k$  of the  $q$  axis at time  $k$  is

$$i_{q\_ref}^k = \frac{\omega_{r\_pre}^{k+1} - (1 + m_1)\omega_r^k + m_1\omega_r^{k-1}}{n_1} + i_q^{k-1} \tag{23}$$

Substituting the given current  $i_{d\_ref}^k = 0$  of the  $d$  axis at time  $k$  into Equation (14), the current given values of the  $\alpha$ - and  $\beta$ -axes at time  $k$  can be obtained.

$$\begin{bmatrix} i_{\alpha\_ref}^k \\ i_{\beta\_ref}^k \end{bmatrix} = \begin{bmatrix} \cos(\theta_e) & -\sin(\theta_e) \\ \sin(\theta_e) & \cos(\theta_e) \end{bmatrix} \begin{bmatrix} i_{d\_ref}^k \\ i_{q\_ref}^k \end{bmatrix} \tag{24}$$

According to the previous equations, the proposed MPC, based on a dual second-order model, was shown in Figure 4, where the current loop and speed loop can be seen using the second order model, shown in Equations (22)–(24).

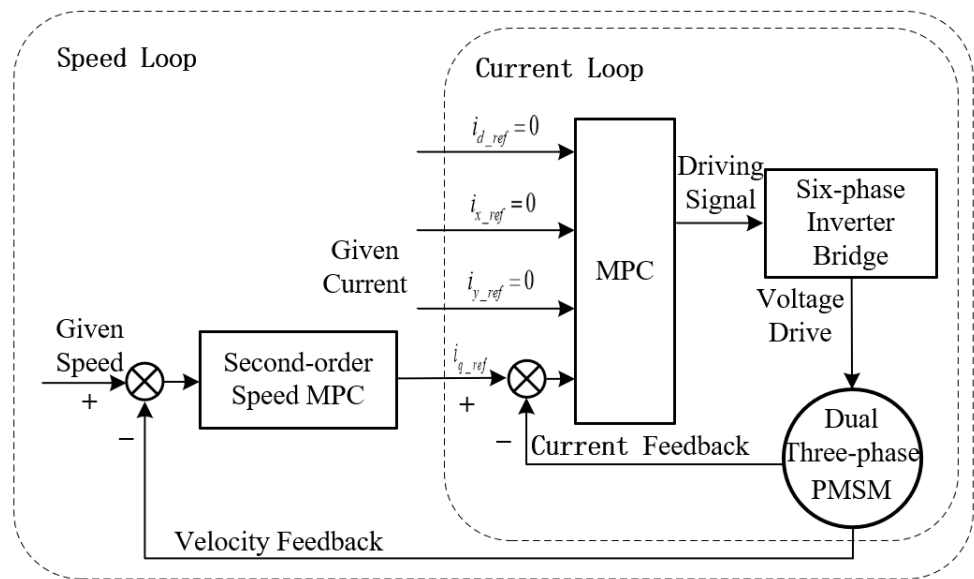


Figure 4. Dual second-order model predictive current control block diagram.

#### 4. Simulation Analysis

To verify the feasibility and validity of the proposed algorithm, the algorithm is verified by Matlab/Simulink. The parameters of the non-salient dual three-phase permanent magnet synchronous motor and the drive system used in the simulation are presented in Table 1.

**Table 1.** Parameters of the motor and drive system.

Parameters	Value
Stator resistance/ $\Omega$	1
Quadrature axis and direct axis inductance /H	0.003
Leakage inductance/H	0.0007
Permanent magnet flux linkage/Wb	0.12
Number of pole pairs	4
Rotational inertia/( $\text{kg}\cdot\text{m}^2$ )	0.01
Rated load torque/( $\text{N}\cdot\text{m}$ )	30
Rated speed/( $\text{r}/\text{min}$ )	1000
Friction coefficient/( $\text{N}\cdot\text{m}\cdot\text{s}$ )	0.0003
Inverter bridge DC bus voltage/V	200

This study compares the responses of four control modes. The information and the corresponding abbreviations of the four control modes are listed in Table 2.

**Table 2.** Control methods and their abbreviations.

Control Methods	Abbreviations
Speed loop P1 + current loop traditional MPC	P1 + traditional MPC
Speed loop P1 + current loop first-order MPC	P1 + first-order MPC
Speed loop P1 + current loop second-order MPC	P1 + second-order MPC
Second-order MPC for both speed loop and current loop	Dual second-order MPC

To compare the results, the principle of a single variable is adopted in this study. Additionally, the maximum four-vector SVPWM is used to modulate the voltage vector for 'PI + traditional MPC' to eliminate the impact on the comparison of simulation results due to different modulation modes.

The initial value of the given speed is 1000 r/min with a no-load start. Then, a rated load of 30 N·m is applied at 0.06 s. Figure 4 illustrates the speed of response of the four control modes. Figure 5 illustrates the torque response of the four control modes. Table 3 presents the performance of the four control modes.

As shown in Figures 5 and 6, and Table 3, for the steady-state situation, the current loops of the 'PI + first-order MPC', 'PI + second-order MPC', and 'dual second-order MPC' control modes all adopt the MPC derived in this study, and these three control modes adjust the direction and amplitude of the output voltage vector. As a result, their steady-state speed fluctuation and torque fluctuation are much smaller than those of the 'PI + traditional MPC' control mode. For transient situations, the current loop adopts the MPC mode, and it has a strong tracking ability to the speed loop. Therefore, the speed response performance is subject to the speed loop adjustment mode. Meanwhile, the adjustment process curves of the speed response and torque response of 'PI + traditional MPC', 'PI + first-order MPC', and 'PI + second-order MPC' approximately overlap, and the performance data are nearly equal. However, the speed loop of 'dual second-order MPC' adopts MPC control. Therefore, it achieves more excellent performance data than the speed loop using PI control, and the speed response is fast with a small overshoot, indicating that its transient performance is stronger.

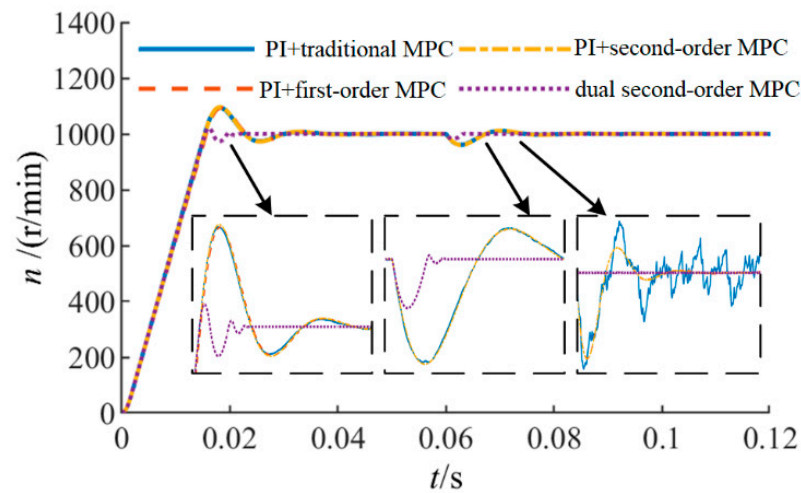


Figure 5. Speed response of four control modes.

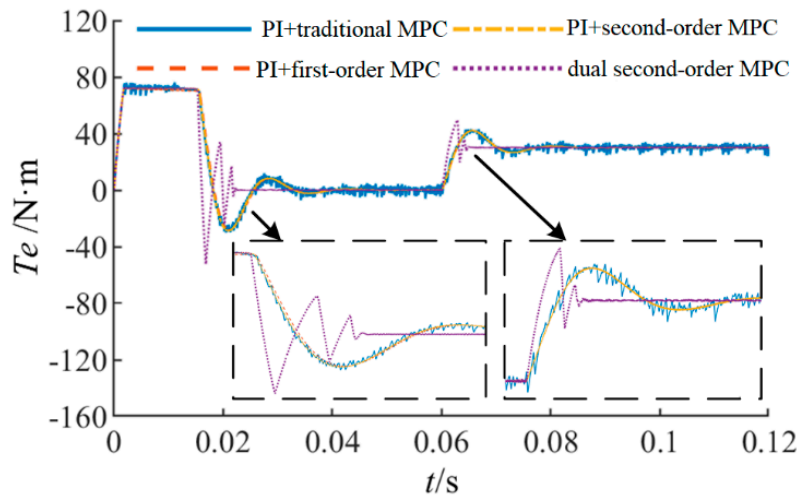


Figure 6. Torque response of four control modes.

Table 3. Performance comparison of the four control modes.

Control Modes	Overshoot / (r/min)	Steady-State Time / ms	Speed Drop / (r/min)	Recovery Time / ms
P1 + traditional MPC	96.5	27.31	40.31	7.24
P1 + first-order MPC	96.2	27.29	40.30	7.24
P1 + second-order MPC	96.3	27.30	40.30	7.23
Dual second-order MPC	21.6	18.88	18.73	4.04

To illustrate the difference in current regulation between the first-order MPC and the second-order MPC of the current loop, Figure 7 shows the comparison of the difference between the given values and the response values of the  $\alpha$ -axis and  $\beta$ -axis currents of ‘P1 + first-order MPC’ and ‘P1 + second-order MPC’, respectively. It can be seen that the difference between the current given value and the response value of ‘P1 + second-order MPC’ is smaller than that of ‘P1 + first-order MPC’, indicating that the former achieves better tracking performance for the given current value than the latter.

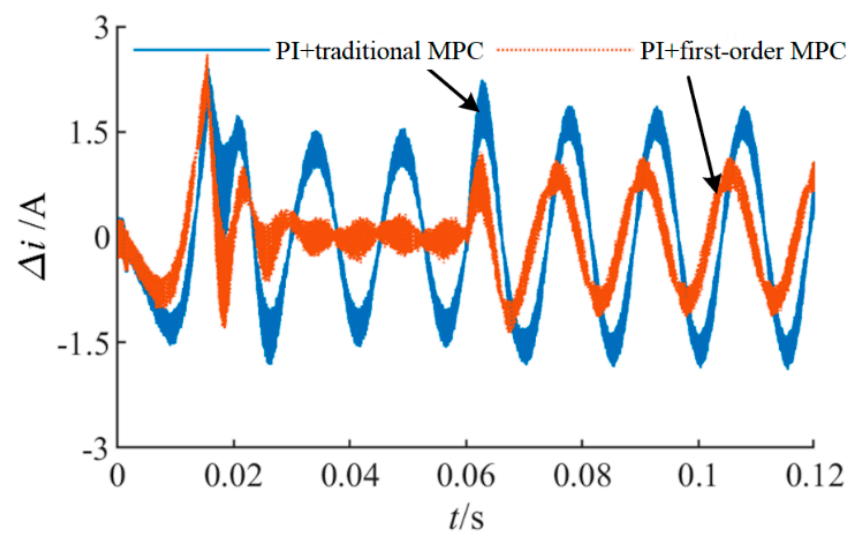
Figure 8 shows the A-phase and U-phase current waveforms of the three current loop MPC control algorithms. After local amplification, the current loop using the traditional MPC algorithm exhibits obvious current ripples, while the current ripples of using the first-order MPC and the second-order MPC are relatively small.

The fundamental amplitude and total harmonic distortion (THD) of the A-phase current in the steady state after adding the load can be calculated through Fourier analysis.

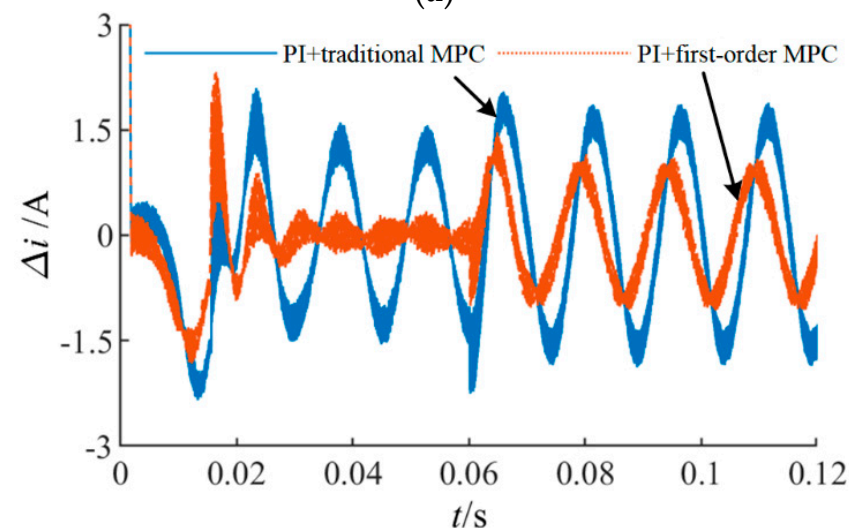
As shown in Table 4, compared to the traditional MPC, the THD of the phase current is significantly reduced in the first/second-order MPC. It indicates that the first/second-order MPC reduces current ripples and harmonics by adjusting the magnitude and direction of the output voltage vector.

**Table 4.** Current analysis of the three current loop control algorithms.

Current Loop Control Modes	Fundamental Amplitude/A	THD/%
Traditional MPC	9.82	17.62
First-order MPC	9.80	3.12
Second-order MPC	9.80	3.11



(a)



(b)

**Figure 7.** Current comparison waveforms of two control modes. (a)  $\alpha$ -axis current comparison; (b)  $\beta$ -axis current comparison.

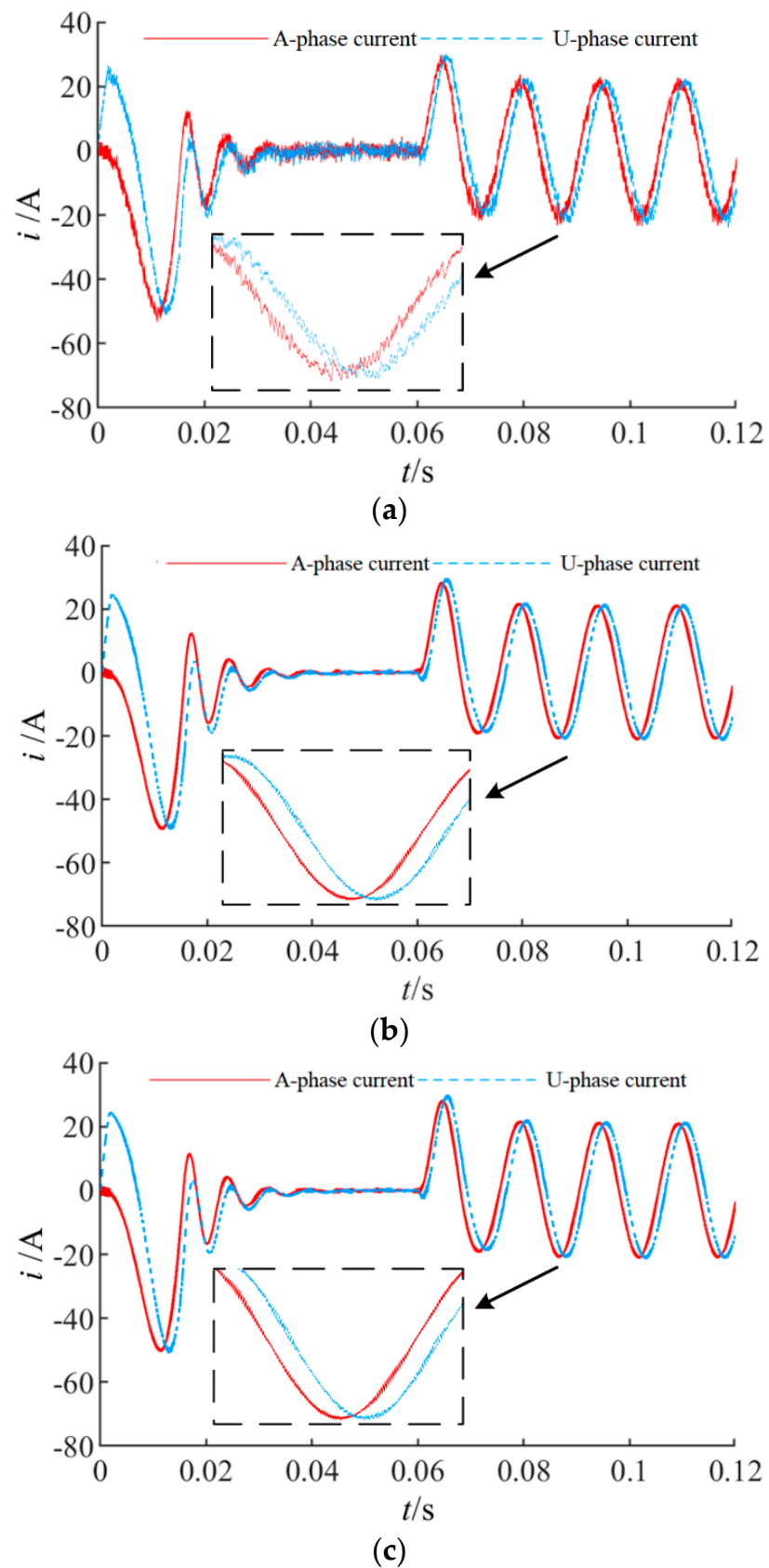


**Figure 8.** Current waveforms of three current loop control algorithms. (a) Traditional MPC in the current loop; (b) First-order MPC in the current loop; (c) Second-order MPC in the current loop.

## 5. Experiment of Dual Second-Order Model Predictive Control Based on Current Loop Optimization

In order to further verify the effectiveness of the proposed algorithm, an experimental platform was built. The experimental platform is shown in Figure 6, which mainly consists of a controller (TI DSP TMS320F28335, Texas, USA); an IGBT switch device (Infineon FF450R17ME4, Germany); a current Hall sensor (LEM CASR15-NP, Swiss); a dynamometer system, which is composed of a tension measurement and control (Zhangli 610L, China); and a magnetic power brake (Zhangli CZ-40, China). High-speed serial communication is used to change the speed command, to read the back EMF and speed information of the motor, and to record the read data; the experiment was recorded with an oscilloscope of Yokogawa DLM3034 and a Zhangli 610L power dynamometer system.

As shown in Table 3, the speed loop effect of 'PI + first-order MPC' is almost the same as that of 'PI + second-order MPC'. Meanwhile, as shown in Table 4 and Figure 6, the current control effect of a second-order MPC in the current loop is also almost the same as that of a first-order MPC in the current loop. Additionally, the current tracking ability of the former is slightly better than that of the latter. Thus three types of control strategies ('PI + traditional MPC', 'PI + second-order MPC', and 'dual second-order MPC') are used for the experiments and comparisons to clearly compare the advantages and disadvantages of using PI or MPC in the speed loop or adopting traditional MPC or the current MPC algorithm proposed in this study in the current loop.

The given speed is 500 r/min with a no-load start. Meanwhile, to reduce the mechanical impact, the given speed is ramped. The speed waveform of each algorithm and the related performance indicators in the start-up process are presented in Figure 9.

As shown in Figure 10, the current loops of 'PI + traditional MPC' and 'PI + second-order MPC' adopt different current MPC control algorithms. However, since the speed loops are limited by PI control, the overshoot and steady-state time of their speed are almost the same. Meanwhile, due to the use of MPC control algorithms, the steady-state time and overshoot of dual second-order MPC are both smaller than the former two. This indicates that, after the speed loop is changed from the PI algorithm to the MPC algorithm, the transient performance of the motor is improved.

After the no-load speed becomes stable, a load torque of 20 N·m is applied. When the speed is stable, the current is collected by the current clamp. Then, the current waveforms of both the traditional MPC and the second-order MPC control algorithm proposed in this study in the current loop are observed through the oscilloscope (Figure 10).

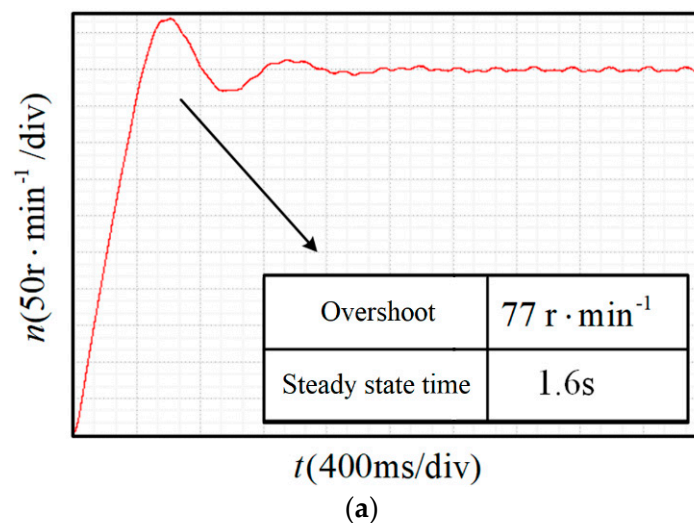
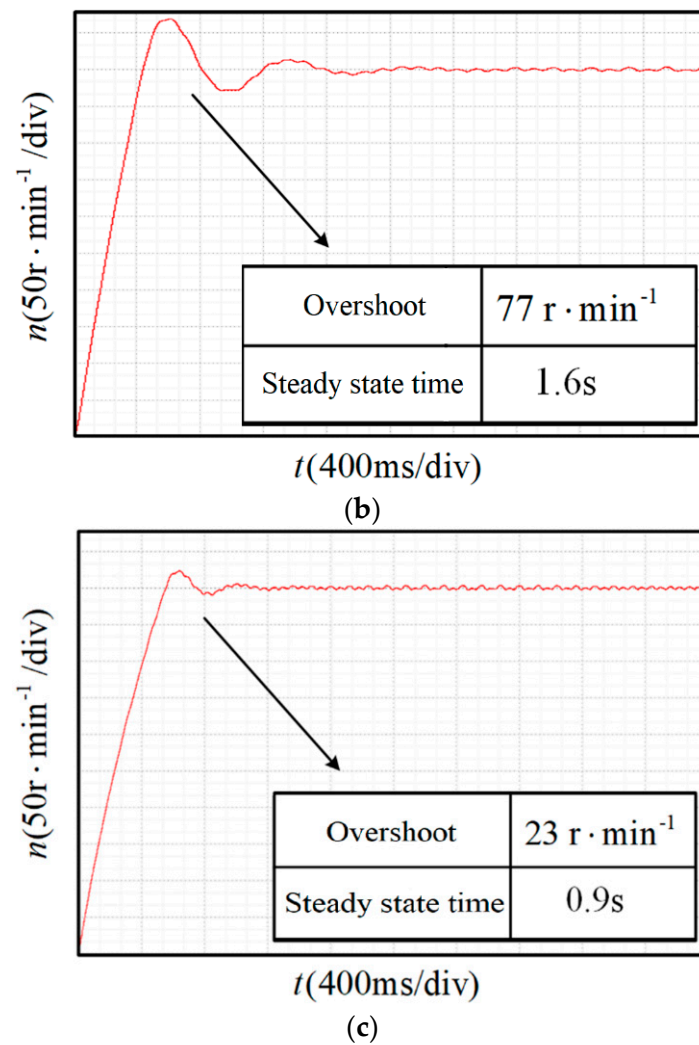
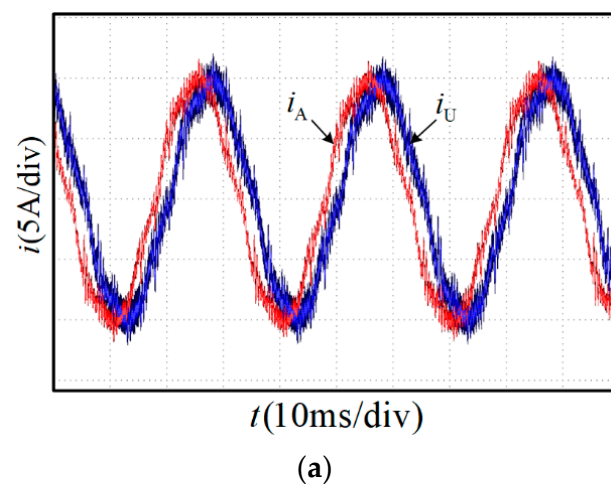


Figure 9. Cont.



**Figure 9.** Speed waveform of each control algorithm. (a) PI + traditional MPC; (b) PI + second-order MPC; (c) Dual second-order MPC.

As shown in Figure 10, the current harmonics controlled by the traditional MPC algorithm in the current loop are relatively large. Obvious current ripples can be observed in Figure 10a. However, the current waveform controlled by the second-order MPC algorithm in the current loop is smoother, which makes the current ripple in Figure 9b smaller.



**Figure 10.** Cont.

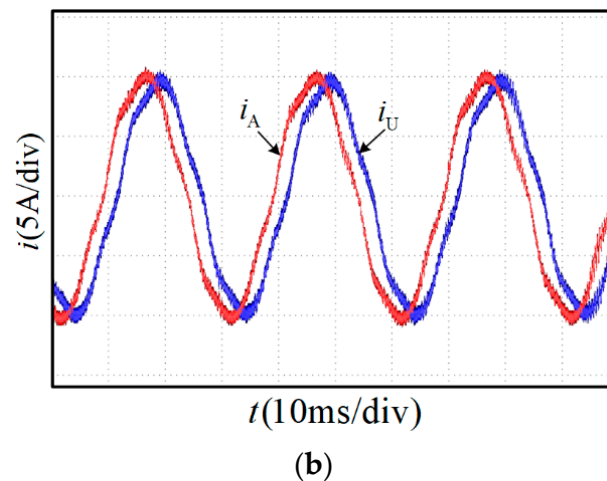


**Figure 10.** Comparison of current waveforms between two MPC control modes.(a) traditional MPC; (b) Dual second-order MPC.

## 6. Conclusions

Based on the traditional MPC adopted in the current loop, this study proposes a dual second-order MPC algorithm based on current loop operation optimization. The second-order MPC is applied to both the speed loop and the current loop. Meanwhile, the maximum four-vector SVPWM is used to modulate the calculated voltage vector. The following conclusions can be obtained:

- (1) The proposed current MPC calculation method can adjust the voltage direction and amplitude at the same time through the voltage vector calculated at one time, which reduces the rotating speed and fluctuations of the current and torque. Additionally, the current tracking of the second-order current MPC is better than that of the first-order current MPC, thus improving the steady-state performance of the motor.
- (2) The speed loop adopts the second-order MPC rotating speed control. The overshoot and adjustment time of the motor speed response is much smaller than that of the PI control, which greatly improves the transient performance of the motor.

According to the simulation and experimental indications, some further research can be conducted on the heavy load and high frequency of PMSM application, and the fast convergence of the MPC algorithm is worth further researching. In practical applications, the performance of MPC is similar to that of traditional proportional control, so the steady-state error should be ensured by the cost function.

**Author Contributions:** Methodology, L.L. and W.Z.; validation, X.B.; formal analysis, X.S. (Xuetao Sun); data curation and writing—original draft preparation, X.S. (Xiaoping Shi). All authors have read and agreed to the published version of the manuscript.

**Funding:** This research received no external funding.

**Data Availability Statement:** Not applicable.

**Conflicts of Interest:** The authors declare no conflict of interest.

## References

1. Xiong, C.; Xu, H.; Guan, T.; Zhou, P. A Constant Switching Frequency Multiple-Vector-Based Model Predictive Current Control of Five-Phase PMSM With Nonsinusoidal Back EMF. *IEEE Trans. Ind. Electron.* **2019**, *67*, 1695–1707. [[CrossRef](#)]
2. Preindl, M.; Bolognani, S. Model Predictive Direct Speed Control with Finite Control Set of PMSM Drive Systems. *IEEE Trans. Power Electron.* **2012**, *28*, 1007–1015. [[CrossRef](#)]
3. Ahmed, A.A.; Koh, B.K.; Lee, Y.I. A Comparison of Finite Control Set and Continuous Control Set Model Predictive Control Schemes for Speed Control of Induction Motors. *IEEE Trans. Ind. Inform.* **2017**, *14*, 1334–1346. [[CrossRef](#)]
4. Zhang, Y.; Yang, H. Model Predictive Flux Control for Induction Motor Drives. In Proceedings of the CSEE, Changsha, China, 23 December 2015; pp. 782–789. (In Chinese)

5. Zedong, Z.; Kui, W.; Yongdong, L.; Hongwei, M. Current Controller for AC Motors Using Model Predictive Control. *Trans. Chin. Electron. Soc.* **2013**, *28*, 118–123. (In Chinese)
6. Yang, H.; Jiang, Y.; Yin, S. Adaptive Fuzzy Fault-Tolerant Control for Markov Jump Systems With Additive and Multiplicative Actuator Faults. *IEEE Trans. Fuzzy Syst.* **2020**, *29*, 772–785. [[CrossRef](#)]
7. Luo, Y.; Liu, C. A Simplified Model Predictive Control for a Dual Three-Phase PMSM With Reduced Harmonic Currents. *IEEE Trans. Ind. Electron.* **2018**, *65*, 9079–9089. [[CrossRef](#)]
8. Luo, Y.; Liu, C. Elimination of Harmonic Currents Using a Reference Voltage Vector Based-Model Predictive Control for a Six-Phase PMSM Motor. *IEEE Trans. Power Electron.* **2018**, *34*, 6960–6972. [[CrossRef](#)]
9. Luo, Y.; Liu, C. Model Predictive Control for a Six-Phase PMSM Motor With a Reduced-Dimension Cost Function. *IEEE Trans. Ind. Electron.* **2019**, *67*, 969–979. [[CrossRef](#)]
10. Sun, X.; Li, T.; Tian, X.; Zhu, J. Fault-Tolerant Operation of a Six-Phase Permanent Magnet Synchronous Hub Motor Based on Model Predictive Current Control With Virtual Voltage Vectors. *IEEE Trans. Energy Convers.* **2021**, 37–49. [[CrossRef](#)]
11. Aciego, J.J.; Prieto, I.G.; Duran, M.J. Model Predictive Control of Six-Phase Induction Motor Drives Using Two Virtual Voltage Vectors. *IEEE J. Emerg. Sel. Top. Power Electron.* **2018**, *7*, 321–330. [[CrossRef](#)]
12. Barrero, F.; Arahal, M.R.; Gregor, R.; Toral, S.; Duran, M.J. A Proof of Concept Study of Predictive Current Control for VSI-Driven Asymmetrical Dual Three-Phase AC Machines. *IEEE Trans. Ind. Electron.* **2009**, *56*, 1937–1954. [[CrossRef](#)]
13. Alhosaini, W.; Diao, F.; Mahmud, M.H.; Wu, Y.; Zhao, Y. A Virtual Space Vector-Based Model Predictive Control for Inherent DC-Link Voltage Balancing of Three-Level T-Type Converters. *IEEE J. Emerg. Sel. Top. Power Electron.* **2020**, *9*, 1751–1764. [[CrossRef](#)]
14. Duran, M.; Barrero, F.; Toral, S.; Arahal, M.; Prieto, J. Improved techniques of restrained search predictive control for multiphase drives. In Proceedings of the IEEE International Electric Machines & Drives (IEMDC), Miami, FL, USA, 3–6 May 2009.